

Effect of Finite Impurity Mass on the Anderson Orthogonality Catastrophe in One Dimension

H. Castella

Institut Romand de Recherche Numérique en Physique des Matériaux (IRRMA),

PHB-Écublens, CH-1015 Lausanne, Switzerland

and

Department of Physics, Ohio State University,

*174 West 18th Ave., Columbus, OH, 43210-1106. **

(Received)

Abstract

A one-dimensional tight-binding Hamiltonian describes the evolution of a single impurity interacting locally with N electrons. The impurity spectral function has a power-law singularity $A(\omega) \propto |\omega - \omega_0|^{-1+\beta}$ with the same exponent β that characterizes the logarithmic decay of the quasiparticle weight Z with the number of electrons N , $Z \propto N^{-\beta}$. The exponent β is computed by (1) perturbation theory in the interaction strength and (2) numerical evaluations with exact results for small systems and variational results for larger systems. A nonanalytical behavior of β is observed in the limit of infinite impurity mass. For large interaction strength, the exponent depends strongly on the mass of the impurity in contrast to the perturbative result.

I. INTRODUCTION

Anderson studied the effect of a static impurity potential on conduction electrons in metals [1] and showed that the groundstate of the electrons is strongly renormalized by the local potential of the impurity and has an overlap with the unperturbed state, or quasiparticle weight Z , vanishing as $Z \propto N^{-\beta}$ with increasing number of electrons N . This effect, known as the Anderson orthogonality catastrophe, has its origin in an infrared singularity due to shake-up processes of the electron sea in the presence of the impurity potential [2] and signals the failure of the quasiparticle picture to describe the low-energy excitations.

The infrared singularity also affects the optical properties of metals. The core-level hole created by an X-ray disturbs the conduction electrons similarly to an impurity potential. On one hand, the X-ray photoemission spectrum is asymmetrically broadened above the threshold [3,4]. On the other hand, the X-ray absorption spectrum has a strongly enhanced threshold, the so-called Fermi-edge singularity [5].

These singularities in the optical spectra apply for a static core hole, i.e., an infinite-mass hole (or impurity). For a finite-mass hole and an isotropic band dispersion, the infrared singularity does not occur in three dimensions because the hole recoil strongly restricts the number of low-energy excitations [6,7]; as a consequence, the edge singularities disappear. In one dimension, however, the infrared singularity persists even for a finite-mass hole [8]. The observation of an enhanced threshold in UV-absorption spectra of doped semiconductor quantum wires was interpreted as a Fermi-edge singularity [9] and stimulated renewed interest in the one-dimensional problem [10,11].

The present work studies the Anderson orthogonality for a finite-mass impurity in a simple one-dimensional model and focusses on the impurity recoil. Although the infrared singularity occurs for both an infinite- and a finite-mass impurity in one dimension, the recoil plays an important role on the critical exponent β which does not extrapolate to the static-impurity value in the infinite-mass limit. The dependence of the exponent on the impurity mass is investigated analytically by perturbation theory and numerically by a variational

approach in the nonperturbative regime. The results are eventually compared to analytical calculations from Ref. [12] which studied the heavy-mass and strong-coupling regime using a path-integral formalism [13].

The next section presents the model and the results. In section III, a perturbation analysis of the impurity spectral function is performed along the line of Ref. [8]. Section IV calculates numerically the critical exponent using a variational approach.

II. MODEL AND RESULTS

This section presents the model and summarizes the known results on the impurity spectral function and the Anderson orthogonality catastrophe. At the end of the section, the main results of this work are briefly described.

The model describes a single impurity and N spinless electrons moving on a chain of L sites with periodic boundary conditions. Within a tight-binding approximation with nearest-neighbor hopping, the band energies are $-2t_h \cos k$ and $-2t \cos k$ for the impurity and the electrons, respectively. Further, the impurity and the electrons feel an interaction U when they sit on the same site. Although this study is restricted to a single impurity, it is convenient to write the Hamiltonian \hat{H} in second-quantized form with creation operators c_i^\dagger for an electron on site i , and d_i^\dagger for an impurity:

$$\hat{H} = -t \sum_{i=1}^L (c_i^\dagger c_{i+1} + h.c.) - t_h \sum_{i=1}^L (d_i^\dagger d_{i+1} + h.c.) + U \sum_{i=1}^L d_i^\dagger d_i c_i^\dagger c_i. \quad (1)$$

The interaction is attractive in order to describe a hole in a valence band. For this particular model, however, the repulsive and attractive cases are related by a particle-hole transformation for the electrons $\tilde{c}_j = (-1)^j c_j^\dagger$. In the rest of the paper all the results are presented for the repulsive case; the corresponding results for the attractive interaction are obtained by the transformation $\rho \rightarrow 1 - \rho$ where $\rho = N/L$ is the density of conduction electrons.

The spectral function of the hole (or impurity) $A(q, \omega)$ describes the photoemission response within the sudden approximation, i.e., neglecting interaction with the outgoing electron [14]. It has a spectral decomposition in terms of eigenstates, $|\psi_n\rangle$, and eigenenergies,

E_n , of the Hamiltonian (1) in presence of the impurity, and of the groundstate wavefunction, $|\phi_0\rangle$, and energy, \tilde{E}_0 , in absence of impurity:

$$A(q, \omega) = \frac{1}{\pi} \text{Im} G_q(\omega) = \sum_n |\langle \psi_n | d_q^\dagger | \phi_0 \rangle|^2 \delta(\omega - E_n + \tilde{E}_0). \quad (2)$$

In the spectral decomposition of $A(q=0, \omega)$, the spectral weight of the groundstate $Z = |\langle \psi_0 | d_{q=0}^\dagger | \phi_0 \rangle|^2$ may remain finite in the thermodynamic limit, giving rise to a quasiparticle peak in the spectral function. This is the usual situation when the quasiparticle picture applies.

Static impurity ($t_h = 0$). The interaction causes the quasiparticle picture to break down [1]: the spectral weight scales to zero with increasing number of fermions N as $Z \propto N^{-\beta}$, the groundstate of the interacting system being orthogonal to the quasiparticle state $d^\dagger | \phi_0 \rangle$ for $N \rightarrow \infty$. This is known as the Anderson orthogonality catastrophe. The exponent is related to the phaseshift δ_F of an electron at the Fermi energy scattered off the static impurity:

$$\beta(t_h = 0) = (\delta_F/\pi)^2. \quad (3)$$

For the present model, the phaseshift depends on U and on the density of states at the Fermi energy $N_F = 1/(2\pi \sin k_F)$: $\delta_F = -\arctan(\pi U N_F)$. Furthermore, the spectral function has, instead of a quasiparticle peak, a power-law singularity at the threshold $\omega_0 = E_0 - \tilde{E}_0$ with the critical exponent $1 - \beta(t_h = 0)$ [4]:

$$A(\omega) \propto \frac{1}{|\omega - \omega_0|^{1-\beta}}. \quad (4)$$

This singularity in $A(\omega)$ is observed in X-ray photoemission of metals [3].

Finite mass impurity ($t_h > 0$). While an infinite-mass impurity acts as an external potential on the electrons, the impurity recoil further complicates the many-body problem. Despite this complexity, the eigenenergies and eigenstates of \hat{H} are known exactly for the special case $t_h = t$ [15]. Using the exact solution, the spectral function for $q \simeq 0$ is computed in Ref. [16]. It has no quasiparticle peak because of the Anderson orthogonality catastrophe and has a power-law singularity with an exponent:

$$\beta(t_h = t) = 2(\delta'_F/\pi)^2 \quad (5)$$

The exponent is given by the phaseshift of a single electron at k_F scattering off a finite-mass impurity $\delta'_F = -\arctan(\pi UN_F/2)$. Notice the similarity in the exponents for $t_h = t$ and $t_h = 0$, which are both expressed in terms of phaseshifts. The phaseshifts, however, differ since the number of states contributing to the Anderson orthogonality is reduced from UN_F to $UN_F/2$ between a static and finite mass impurity, respectively. The origin of this difference is discussed in Section III for the perturbative results.

The present work presents calculations of the exponent $\beta(t_h)$ for different hopping parameters t_h , interaction strengths U , and electron densities ρ . The exponent $\beta(t_h)$ is computed (1) analytically using perturbation theory in U and (2) numerically in the nonperturbative regime using a variational wavefunction proposed by Edwards [17]. The exponent is extracted numerically from finite size results using a precise scaling law for Z as a function of N and a numerical fit of the data as $N \rightarrow \infty$. The main results of this study are summarized now. Sections III and IV will give a detailed description of the perturbation calculations and the numerical simulations, respectively.

Mass dependence of the exponent. The perturbative results indicate that the exponent β , to order $(U/t)^2$, is independent of t_h for $t_h > 0$ and equals $(UN_F)^2/2$. For a finite U , however, the exponent $\beta(t_h)$ calculated numerically does depend on t_h and its dependence increases with increasing U , as illustrated in Fig. 1 that shows the exponent normalized to its value for $t_h = t$, $\beta(t_h)/\beta(t_h = t)$, as a function of t_h . In the strong coupling limit, $U = \infty$, β varies quasi linearly with t_h .

Discontinuous exponent in the heavy-mass limit. The perturbative calculations predict a discontinuous exponent in the limit of a flat impurity dispersion: $\lim_{t_h \rightarrow 0} \beta(t_h) = \beta(t_h = 0)/2$. This discontinuity is due to the irrelevance of backscattering processes for $t_h > 0$ because of the finite recoil energy involved. The numerical results in Fig. 1 illustrate the nonanalyticity for a finite U : when $t_h \rightarrow 0$ the exponent does not extrapolate to the static value which is indicated by the filled symbols at $t_h = 0$. The numerical results can be

compared to calculations of A. Rosch and T. Kopp [12] for the exponent in the heavy-mass and strong-coupling regime. Their analysis, based on an effective action for the long-time behavior of the impurity propagator, also predicts a discontinuity $\lim_{t_h \rightarrow 0} \beta(t_h)/\beta(t) = \alpha \neq \beta(0)/\beta(t)$ and gives at half filling $\alpha = 1/4$ while at third filling $\alpha = 19/56 \simeq 0.339$. The numerical results in Fig. 1 suggest $\alpha \simeq 0.25$ for both half and third filling. The result at half filling is therefore in good agreement with their prediction while at third filling the value of α is significantly smaller. Note however that the present work relies on a variational approach.

Crossover behavior in the heavy-mass limit. A detailed analysis of the perturbative results for $t_h \ll t$ reveals a crossover in the scaling behavior of $\ln Z$ as a function of $\ln N$, as shown in Fig. 2. While $\ln Z$ closely follows the static-impurity behavior with a slope $\beta(t_h = 0)$ for a number of fermions smaller than a crossover value N_c , it adjusts to the finite-mass behavior only for $N > N_c$. Further N_c diverges as t/t_h for $t_h \rightarrow 0$. Therefore, the discontinuity is only an asymptotic result, valid in the limit $N \rightarrow \infty$.

III. PERTURBATION THEORY

This section evaluates the impurity spectral function and spectral weight Z perturbatively in U and for an arbitrary hopping parameter t_h in one dimension, following Ref. [8] that computes $A(q = 0, \omega)$ for the equal-masses case ($t_h = t$) in connection with the stability of the ferromagnetic state in the Hubbard model.

Spectral weight. In the perturbative expansion, the first terms that renormalize the ground-state wavefunction correspond to the creation of a single particle-hole pair within the Fermi sea by an impurity of momentum $q = 0$. The excitation energy is: $\Delta\epsilon(k_1, k_2) = 2t \cos k_1 - 2t \cos k_2 + 2t_h - 2t_h \cos(k_1 - k_2)$. The spectral weight has a cumulant expansion [6] that, up to second order in U , involves only these excitations:

$$\ln Z = - \left(\frac{U}{L}\right)^2 \sum_{k_1, k_2} \frac{\Theta(k_F - |k_1|)\Theta(|k_2| - k_F)}{\Delta\epsilon(k_1, k_2)^2}. \quad (6)$$

The sum over k_1, k_2 diverges logarithmically with increasing number of electrons N . As shown in the Appendix, a large N expansion gives :

$$\ln Z = -\beta(t_h) \ln N + \alpha_0(t_h) + \alpha_1(t_h)/N + O(1/N^2). \quad (7)$$

The logarithmic term dominates for large N and gives rise to the Anderson orthogonality. The finite-size corrections are used in Section IV for the numerical study of β .

The main result of this section is the evaluation of $\beta(t_h)$:

$$\begin{aligned} \beta(0) &= (UN_F)^2 \quad \text{for } t_h = 0 \\ \beta(t_h) &= \frac{1}{2}(UN_F)^2 \quad \text{for } t_h > 0 \end{aligned} \quad (8)$$

The exponent $\beta(t_h)$ is independent of t_h as far as $t_h > 0$. The infrared singularity is caused by forward-scattering processes with small momentum transfer $|k_2 - k_1| \ll k_F$, which are gapless excitations for any t_h . The hopping t_h is irrelevant since the impurity recoil energy $2t_h(\cos(k_1 - k_2) - 1)$ is negligible as compared to the particle-hole energy $2t(\cos k_2 - \cos k_1)$.

Further, the exponent has a discontinuity in the heavy-mass limit $\lim_{t_h \rightarrow 0} \beta(t_h) = \beta(t_h = 0)/2$. The difference between the infinite- and the finite-mass exponents is simply related to scattering of one electron from one side of the Fermi surface to the other. These so-called backscattering processes, which involve a large momentum transfer $|k_2 - k_1| \simeq 2k_F$, do not contribute to the infrared divergence for $t_h > 0$ since the impurity recoil opens a gap $2t_h(\cos 2k_F - 1)$. For $t_h = 0$ however, both backscattering and forward-scattering processes are gapless. The number of low-energy excitations contributing to the infrared singularity is thus reduced by a factor of 2 for a finite-mass impurity as compared to its value for the static impurity.

The discontinuity in the exponent is an asymptotic result valid only for $N \rightarrow \infty$. For a finite number of fermions and a large but finite mass $0 < t_h \ll t$ however, $\ln Z$ has a crossover as a function of $\ln N$, illustrated in Fig. 2 where the spectral weight is computed numerically from (6). The logarithm of the spectral weight has the slope $\beta(t_h)$ only for a number of electrons larger than a crossover value N_c , while for a small N it follows the

static-impurity behavior with a slope $\beta(t_h = 0)$. The dashed lines indicate the asymptotic behaviors $-\ln Z = \beta(t_h) \ln N - \alpha_0(t_h)$, with the analytical β from (8) and α_0 fitted to the value of $\ln Z$ for the largest size. The intercept of the asymptotes gives the crossover size N_c , which agrees very well with the estimate $N_c \simeq 0.3244t/t_h$, presented in the Appendix. Notice that N_c diverges as t/t_h for $t_h \rightarrow 0$ and the asymptotic regime is reached for a larger number of electrons the lower t_h .

Spectral function. The spectral function is computed only at $q = 0$ where it has a power law singularity. The propagator is:

$$G_{q=0}(\tau) = -i \langle \phi_0 | d_{q=0} \exp(-i\hat{H}\tau) d_{q=0}^\dagger | \phi_0 \rangle e^{i\tilde{E}_0\tau} \Theta(\tau). \quad (9)$$

The propagator has also a cumulant expansion and is written in terms of the density of particle-hole excitations $S(\omega)$ and a renormalized impurity energy $\tilde{\epsilon}_0$:

$$G_{q=0}(\tau) = -i \exp \left[-i\tilde{\epsilon}_0\tau - U^2 \int_0^\infty S(\omega) \frac{1 - \exp(-i\omega\tau)}{\omega^2} d\omega \right]. \quad (10)$$

$$S(\omega) = \frac{1}{(2\pi)^2} \int_{-\pi}^\pi \int_{-\pi}^\pi \Theta(|k_1| - k_f) \Theta(k_f - |k_2|) \delta(\omega - \Delta\epsilon(k_1, k_2)) dk_1 dk_2.$$

The density S has a linear frequency dependence for small ω : $S(\omega) = (\beta(t_h)/U^2)\omega$ where $\beta(t_h)$ is the exponent of the Anderson orthogonality in (8). This linear behavior determines the low-frequency spectral function which has a power-law singularity at threshold with the exponent $1 - \beta$ [4]:

$$A(q = 0, \omega) = \frac{\sin(\pi\beta)\Gamma(1 - \beta)}{\pi(\omega - \tilde{\epsilon}_0)^{1-\beta}} \Theta(\omega - \tilde{\epsilon}_0). \quad (11)$$

This is however only an asymptotic result for frequencies smaller than a cutoff W . For $t_h = 0$, the cutoff is of the order of the Fermi energy: $W \simeq 2t(1 - \cos k_F)$. For $t_h > 0$ however, the linear behavior of S holds only for frequencies smaller than the impurity recoil energy and the cutoff is given by $W \simeq \min(2t(1 - \cos k_F), 2t_h(1 - \cos 2k_F))$. For a heavy impurity the cutoff is of the order of the impurity recoil energy $t_h(1 - \cos 2k_F)$ rather than the Fermi energy and the asymptotic result is valid only in a very narrow frequency range.

Furthermore, the density of excitations exhibits a crossover similarly to the spectral weight. This might give rise to a crossover in the spectral function as well.

In summary the exponent β in (8) characterizes the power-law singularity of the spectral function and the logarithmic decay of the quasiparticle weight. The exponent does not depend on the mass of the impurity except in the static limit $t_h = 0$ and it has a discontinuity at $t_h = 0$. Notice that the perturbative results agree with the the small- U expansions of the exponent for $t_h = 0$ and $t_h = t$.

IV. NUMERICAL STUDY

This section presents a numerical study of the exponent $\beta(t_h)$ based on a variational approach. The variational predictions for the energy and correlation functions are compared to results from Lanczos exact diagonalizations and Projection Quantum Monte Carlo simulations. Then the variational calculations are used to extract the exponent.

The variational wavefunction was originally proposed for the single spin-flip problem in the 2D-Hubbard model in reference to the stability of the ferromagnetic state [17]. It was also used to study numerically the quasiparticle weight in two dimensions [18]. Furthermore, this variational approach is equivalent to the approximation used in Ref. [11]. In one dimension, the variational class of wavefunctions contains all the eigenstates of the model (1) for $t_h = t$, as shown by Edwards [17]. The variational approach is thus expected to include much of the relevant correlations even for $t_h \neq t$.

In the reference frame comoving with the impurity a wavefunction $|\Psi_q\rangle$ of total momentum q is represented by a function $f(j_1, \dots, j_N)$ depending only on the positions of the electrons:

$$|\Psi_q\rangle = \frac{1}{\sqrt{L}} \sum_{j_0=1}^L e^{iqj_0} d_{j_0}^\dagger \sum_{j_1, \dots, j_N=1}^L f(j_1 - j_0, \dots, j_N - j_0) c_{j_1}^\dagger \dots c_{j_N}^\dagger |0\rangle. \quad (12)$$

The variational ansatz for f is a determinant of single-particle wavefunctions ϕ_m :

$$f(j_1, \dots, j_N) = \frac{1}{\sqrt{N!}} \det [\phi_m(j_l)]_{m,l=1, \dots, N}. \quad (13)$$

The expectation value of the energy is:

$$\begin{aligned} \langle \hat{H} \rangle = \sum_{l=1}^N & \left[-t \sum_{j=0}^{L-1} (\phi_l^*(j) \phi_l(j+1) + c.c.) + U |\phi_l(0)|^2 \right] \\ & - t_h [\exp(-iq) \det(\mathbf{S}) + c.c.]. \end{aligned}$$

$$\mathbf{S}_{mn} = \sum_{j=0}^{L-1} \phi_m^*(j+1) \phi_n(j). \quad (14)$$

The variational parameters $\phi_m(j)$ are found by minimization of the energy using a steepest descent algorithm. If one chooses as starting $\phi_l(j)$ the exact solution for $t_h = t$, convergence is reached after a relatively small number of iterations even for hopping parameters very different from t .

Comparison of variational results to Lanczos exact diagonalizations and Projection Quantum Monte Carlo simulations. Only small systems are accessible by exact diagonalization because the dimension of the Hilbert space increases very rapidly with the number of lattice sites. For the half-filled band, the biggest closed-shell system studied has $L = 22$ whereas for $\rho = 1/4$ it has $L = 20$. For larger systems, Monte Carlo simulations are required.

Projection Quantum Monte Carlo gives a statistical estimate of ground-state expectation values of observables \hat{O} by a projection of a trial wavefunction $|\psi_T\rangle$ onto the groundstate with the operator $\exp(-\eta\hat{H})$ [19]:

$$\langle \psi_0 | \hat{O} | \psi_0 \rangle = \lim_{\eta \rightarrow \infty} \frac{\langle \psi_T | \exp(-\eta\hat{H}) \hat{O} \exp(-\eta\hat{H}) | \psi_T \rangle}{\|\exp(-\eta\hat{H})|\psi_T\rangle\|^2}. \quad (15)$$

The algorithm used here closely follows Ref. [20]. The imaginary time evolution $\exp(-\eta\hat{H})$ is performed sequentially for small time intervals $\Delta\tau$ and a Trotter decomposition is used for the kinetic-energy and the interaction terms in the Hamiltonian. Eventually the two-body term is represented by discrete Hubbard-Stratonovitch fields that mediate the interaction. For the present calculations a rather large $\eta = 15$ is necessary in order to converge the relevant correlation functions, and the results are extrapolated to $\Delta\tau \rightarrow 0$ using several values of the time interval.

The energy is computed for the groundstate, which has zero total momentum. The relevant quantity is the correlation energy $e_c = E_0 - \tilde{E}_0 - U\rho$ where E_0 and \tilde{E}_0 are the

interacting and noninteracting energy, respectively. Notice that e_c is of order 1 while E_0 is of order N . Table I gives e_c for several system sizes at half and quarter filling and for an interaction equal to the bandwidth $U = 4t$ and a hopping parameter $t_h = 0.5t$. The variational ansatz is not exact for $t_h \neq t$ since the variational energy departs significantly from the exact energy. Nevertheless it remains always very close to the ground-state energy. The relative difference between the exact and the variational energy remains smaller than 0.1% even when extrapolating to the infinite-system limit with a $1/N$ scaling law. For the sake of comparison the correlation energy for the unrestricted Hartree-Fock solution is $-0.4380t$ at quarter filling, a value much larger than the variational energy $-0.6413t$.

The $k = 0$ component of the momentum distribution function of the impurity $n(k = 0)$ has the same scaling law as Z when the Anderson orthogonality catastrophe occurs. Both Z and $n(k = 0)$ are computed in order to test the relevance of the variational calculations to extract the exponent β . Figure 3 shows the ratio of the exact momentum distribution $n(k = 0)$, calculated by either exact diagonalization or Quantum Monte Carlo depending on the system size, to the variational estimate $n(k = 0)_{var}$ as a function of $1/N$ at quarter and half filling, for $U = 4t$ and $t_h = 0.5t$. If the variational result reproduced correctly the scaling behavior of $n(k = 0)$ with N , the ratio $n(k = 0)/n(k = 0)_{var}$ should be constant as a function of $1/N$. At half filling, the ratio remains indeed always close to 1 and the variational approach seems to correctly describe the scaling behavior. At quarter filling however, the comparison relies mostly on Monte Carlo simulations where the estimate of $n(k = 0)$ has strong statistical fluctuations for large system sizes, large autocorrelation times having an essential contribution to the error bars. The comparison to the variational results is therefore delicate but still the ratio remains close to 1 within the error bars. Finally exact-diagonalization results for Z are presented in Fig. 4 for $U = \infty$, $\rho = 1/2$ and different t_h . The slope of $\ln Z$ as a function of $\ln N$ is an estimate of the exponent β and both exact-diagonalization results and variational calculations are in good agreement. These last results illustrate the robustness of the variational wavefunction even in the strong-coupling regime.

Finite-size scaling analysis of the exponent. The finite size corrections to the Anderson orthogonality catastrophe in (7), which were derived from the perturbative analysis, are used now to extract numerically the exponent. It should be stressed that these $1/N$ corrections contrast with the slowly decaying $\ln \ln N$ corrections expected for the paramagnetic phase of the 1-D Hubbard model [21].

The exponent is extracted from numerical data on finite systems by scaling the slope of $\ln Z$ as a function of $\ln N$: the spectral weights Z_1 and Z_2 are computed for systems with a number of fermions N_1 and N_2 , respectively, at a fixed density and a fixed ratio $r = N_1/N_2$; from the perturbative analysis in (7), the slopes $(\ln Z_1 - \ln Z_2)/(\ln N_2 - \ln N_1)$ have a polynomial expansion in $1/\bar{N}$, \bar{N} being the mean number of electrons $\bar{N} = (N_1 + N_2)/2$:

$$\frac{\ln Z_1 - \ln Z_2}{\ln N_1 - \ln N_2} = -\beta + \alpha_1 \frac{1-r^2}{2r \ln r} \frac{1}{\bar{N}} + O\left(\frac{1}{\bar{N}^2}\right). \quad (16)$$

The exponent β is estimated by a numerical fit of the slopes as $\bar{N} \rightarrow \infty$. In practice, it is not possible to keep the ratio N_1/N_2 exactly fixed while increasing \bar{N} but the number of electrons can be adjusted such that N_1/N_2 approaches a fixed value for large \bar{N} . All the results presented here have been obtained for $N_1/N_2 \simeq 0.7$.

The scaling procedure is tested both in the perturbative regime for different t_h and at finite U for $t_h = t$, where β is known analytically. Figure 5 illustrates the scaling procedure for the perturbative regime where $\ln Z$ is computed from (6). The inset shows that the scaling procedure is well behaved even for very large \bar{N} . Furthermore, the scaling analysis is essential to determine the dependence of β on t_h since the finite-size corrections differ in both sign and magnitude for different t_h . Note also that the non-linear terms in $1/\bar{N}$ become increasingly important with decreasing t_h . The spectral weight Z is computed numerically for $t_h = t$ and different U using the Bethe's ansatz wavefunction (13) and the results are fitted with a third-order polynomial in $1/\bar{N}$. The relative accuracy of the fitting procedure in extracting β remains of the order of 10^{-4} even for a strong interaction $U = 8t$, as illustrated in Fig. 6. Although the scaling behavior was derived in the perturbative regime, it seems to hold for any interaction strength U .

For a finite U and $t_h \neq t$, the exponent is not known and its evaluation relies on the variational approach and the finite-size scaling analysis. Figure 7 illustrates the scaling procedure in the strong-coupling regime $U = \infty$, for $\rho = 1/2$ and different t_h . For $t_h > 0.1t$, the exponent, which is obtained by an extrapolation of the data as $N \rightarrow \infty$, depends only slightly on the order of the polynomial used in the fit. For $t_h = 0.1t$, however, the fitting procedure is not well-behaved and a relative error of a few percents is expected in the extraction of β . A precise investigation of the heavy-mass regime $t_h \ll t$ would require the study of even larger systems due to the important nonlinear corrections in $1/N$.

Mass dependence of the exponent. The study of $\beta(t_h)$ is based on the variational approach and the scaling analysis presented above. Figure 1 presents the exponent normalized to its value at $t_h = t$, $\beta(t_h)/\beta(t_h = t)$, as a function of t_h/t . For a finite U , the exponent does depend on the hopping parameter t_h , in contrast to the perturbative result $\beta(t_h)/\beta(t_h = t) = 1$ indicated by the dotted line. Furthermore, this dependence increases with increasing U and in the strong-coupling regime $U = \infty$ the exponent varies quasi-linearly with t_h/t . For small t_h and at half filling, the exponent only slightly departs from the linear behavior. Furthermore, the exponent depends on the density since the data for $U = \infty$ and $\rho = 1/2$ significantly differ from the exponents for $\rho = 1/3$. This contrasts with the exact exponent for $t_h = 0$ and $t_h = t$ which are independent of the density. However, the limiting value $\lim_{t_h \rightarrow 0} \beta(t_h)$ seems independent of the density.

The numerical results demonstrate the discontinuity of the exponent at $t_h = 0$ for a finite U . The numerical data, indeed, do not extrapolate to the exact results for $t_h = 0$ indicated by the filled symbols in Fig. 1. A precise extraction of the limiting value $\lim_{t_h \rightarrow 0} \beta(t_h)$, however, would require the investigation of larger systems.

The occurrence of the nonanalyticity at $t_h = 0$ is not surprising since the translational symmetry is broken at this point. Still the role played by the recoil of the impurity in the discontinuity of the exponent is not clear. The perturbation calculations indicate that the discontinuity at $t_h = 0$ is due to the irrelevance of the backscattering processes whenever $t_h > 0$; yet a simple argument can persuade us that this is true only in the small U regime.

Indeed let us assume first backscattering to be responsible for the nonanalyticity for all U . One can devise an effective model for the heavy-impurity limit ($t_h \ll t$) where the impurity is considered static but the interaction with the electrons is restricted to forward scattering :

$$H = -2t \sum_k \cos k c_k^\dagger c_k + \frac{U}{L} \sum_{kk' > 0} c_k^\dagger c_{k'}. \quad (17)$$

In this picture, the only effect of the impurity recoil is the restriction to forward-scattering processes. Since the potential is static, the exponent is expressed in terms of phaseshifts. A calculation of the phaseshift gives the same exponent as the result for $t_h = t$ in (5). This is not compatible with the numerical results for $t_h \ll t$. Therefore forward-scattering processes alone cannot account for the discontinuity and backscattering has to be invoked.

V. CONCLUSIONS

This study of the one-dimensional Anderson orthogonality catastrophe, combining analytical and numerical calculations, has focussed on the effect of the impurity recoil.

The numerical study requires a finite-size scaling analysis since the Anderson orthogonality catastrophe results from a logarithmic decay of the quasiparticle weight with the number of fermions. The present work shows, however, that a reliable numerical analysis of the quasiparticle renormalization can be achieved if a precise scaling hypothesis is established and large enough systems are accessed.

Within perturbation theory, the infrared singularity that signals the orthogonality catastrophe occurs for an impurity band of any dispersion. Still, there is a discontinuity between the zero-bandwidth exponent and the finite-bandwidth exponent. This discontinuity is related to the impurity recoil which opens a gap in the spectrum of particle-hole excitations for backscattering of one electron from the Fermi momentum k_F to $-k_F$.

Outside of the perturbative regime, the numerical analysis demonstrates the discontinuous behavior of the exponent and agrees at half filling with a study of the heavy-mass and strong-coupling regime in Ref. [12]. At third filling however, the numerical results differ from the analytical prediction.

The discontinuity of the exponent is an asymptotic result valid only in the limit of an infinite system. For a finite number of electrons and a heavy but finite-mass impurity the quasiparticle weight has the same logarithmic behavior as a static impurity up to a critical number of electrons N_c where the former weight shows a crossover to the true asymptotic decay for a finite-mass impurity. Furthermore, N_c diverges with increasing mass of the impurity. This crossover is also expected in the low-frequency behavior of the spectral function.

ACKNOWLEDGMENTS

I would like to thank X. Zotos, R. Car and J. Wilkins for their great help and support, as well as T. Kopp and A. Rosch for useful discussions. This work was supported at the institute IRRMA by the Swiss National Science Foundation and the University of Geneva, and at the Ohio State University by a young investigator grant from the Swiss National Science Foundation and by the DOE - Basic Energy Sciences, Division of Material Sciences.

APPENDIX:

This appendix derives the scaling law (7) from the perturbative expression of the spectral weight Z and estimates the crossover size N_c . The calculations are presented for the half-filled band in details and the density dependence of N_c is briefly discussed at the end.

Forward scattering processes. An electron with momentum k_1 is scattered into an empty state with momentum k_2 such that $k_1 k_2 > 0$. The infrared singularity is caused by excitations around the Fermi momentum $k_F = \pi/2$ whose energy vanishes linearly with the momentum transfer $k_1 - k_2$. For k_1 and $k_2 > 0$, the momenta are written as $k_1 = k_F - 2\pi n_1/L$, $k_2 = k_F + 2\pi n_2/L$ and the excitation energy is:

$$\Delta\epsilon(k_1, k_2) \simeq 4\pi t \frac{n_1 + n_2}{2N} \left(1 + \frac{t_h \pi (n_1 + n_2)}{2Nt} \right). \quad (\text{A1})$$

While the linearization of the energies allows an exact calculation of the exponent $\beta(t_h)$, it provides only an estimation of the remaining terms in (7). The contribution of forward-scattering processes to the spectral weight is:

$$-\left(\frac{U}{L}\right) \sum_{k_1 k_2 > 0} \frac{1}{\Delta\epsilon(k_1, k_2)^2} = -\frac{1}{2}(UN_F)^2 \sum_{n_1=0}^{N/2} \sum_{n_2=1}^{N/2} \frac{1}{(n_1 + n_2)^2 (1 + \pi t_h (n_1 + n_2)/(2Nt))^2}. \quad (\text{A2})$$

The fraction in the sum is expanded in four different terms:

$$\frac{1}{(n_1 + n_2)^2 (1 + \pi t_h (n_1 + n_2)/(2Nt))^2} = \frac{1}{(n_1 + n_2)^2} + \frac{1}{(n_1 + n_2 + 2Nt/(\pi t_h))^2} - \frac{\pi t_h}{Nt(n_1 + n_2)} + \frac{\pi t_h}{Nt(n_1 + n_2 + 2Nt/(\pi t_h))}. \quad (\text{A3})$$

The first term gives the logarithmic divergence [22]:

$$\sum_{n_1=0}^{N/2} \sum_{n_2=1}^{N/2} \frac{1}{(n_1 + n_2)^2} = \ln N + 1 + C - 2 \ln 2 + \frac{1}{N} + O\left(\frac{1}{N^2}\right). \quad (\text{A4})$$

where $C \simeq 0.5772$ is Euler's constant. The contributions of all other terms remain finite for $N \rightarrow \infty$. For the second and fourth terms in (A3), the discrete sum can be replaced by an integral. Further the finite-size corrections are of order $1/N$. The extraction of the finite-size corrections for the third term, however, requires the evaluation of the discrete sum: [22]:

$$\frac{1}{N} \sum_{n_1=0}^{N/2} \sum_{n_2=1}^{N/2} \frac{1}{n_1 + n_2} = \ln 2 + \left(\ln 2 - \frac{1}{2}\right) \frac{1}{N} + O\left(\frac{1}{N^2}\right). \quad (\text{A5})$$

Backscattering processes. The initial and final momenta have a different sign, $k_1 k_2 < 0$ and, for $k_1 > 0$ and $k_2 < 0$, the momenta are written as $k_1 = k_F - 2\pi n_1/L$ and $k_2 = -k_F - 2\pi n_2/L$. The linearized excitation energy is:

$$\Delta\epsilon(k_1, k_2,) = 4 \left(t_h + \frac{t\pi(n_1 + n_2)}{2N} \right). \quad (\text{A6})$$

For $t_h = 0$, backscattering processes are gapless excitations and have the same contribution to Z as forward-scattering processes, as given in (A4). For $t_h > 0$, however, they have a gap and their contribution, which is finite, is computed by an integral representation of the sum.

Finally, all the terms, for both forward-scattering and backscattering, give finite size corrections of order $1/N$. Furthermore the coefficient α_0 in (7) is evaluated explicitly in order to extract the crossover size N_c :

$$\alpha_0(t_h = 0) = -\beta(0) (1 + C - 2 \ln 2). \quad (\text{A7})$$

$$\alpha_0(t_h > 0) = -\beta(t_h) \left[1 + C + \ln \frac{2t(\pi t_h + 2t)}{(\pi t_h + 4t)^2} + \frac{\pi t_h}{t} \ln \frac{\pi t_h + 2t}{\pi t_h + 4t} + \ln \frac{(\pi t + 4t_h)^2}{8t_h(\pi t + 2t_h)} \right]. \quad (\text{A8})$$

The crossover size N_c is the solution of the equation:

$$-\beta(0) \ln N_c + \alpha_0(0) = -\beta(t_h) \ln N_c + \alpha_0(t_h) \quad (\text{A9})$$

The crossover occurs for $t_h \ll t$ where $\alpha_0(t_h)$ is diverging logarithmically. As a consequence N_c is proportional to t_h/t :

$$N_c = \frac{\pi t}{2t_h} \exp(-1 - C) \simeq 0.3244 \frac{t}{t_h}. \quad (\text{A10})$$

Arbitrary density. The scaling law (7) applies to any density. Furthermore the crossover size is proportional to t/t_h and diverges as $1 - \rho$ in the limit $\rho \rightarrow 1$.

REFERENCES

* Present address.

- [1] P. W. Anderson, Phys. Rev. Lett. **18**, 1049 (1967); Phys. Rev. **164**, 352 (1967).
- [2] J. J. Hopfield, Com. Solid State Phys. **2**, 40 (1969).
- [3] G. K. Wertheim and P. H. Citrin, in *Photoemission in Solids II*, ed. L. Ley, M. Cardona (Springer, Berlin, 1979); for a review see K. Ohtaka and Y. Tanabe, Rev. Mod. Phys. **62**, 929 (1990).
- [4] S. Doniach and M. Sunjić, J. Phys. C **3**, 285 (1970).
- [5] G. D. Mahan, Phys. Rev. **163**, 612 (1967), P. Nozières, J. Gavoret, and B. Roulet, Phys. Rev. **178**, 1084 (1969), P. Nozières and C. T. DeDominicis, Phys. Rev. **178**, 1097 (1969).
- [6] E. Müller-Hartmann, T. V. Ramakrishnan, and G. Toulouse, Phys. Rev. B **3**, 1102 (1971).
- [7] J. Gavoret, P. Nozières, B. Roulet, and M. Combescot, J. Phys. (Paris) **30**, 987 (1969), S. Doniach, Phys. Rev. B **2**, 3898 (1970), A. E. Ruckenstein and S. Schmitt-Rink, Phys. Rev. B **35**, 7551 (1987).
- [8] T. Kopp, A. E. Ruckenstein, and S. Schmitt-Rink, Phys. Rev. B **42**, 6850 (1990).
- [9] J. M. Calleja, A. R. Goñi, B. S. Dennis, J. S. Weiner, A. Pinczuk, S. Schmitt-Rink, L. N. Pfeiffer, K. W. West, J. F. Müller, and A. E. Ruckenstein, Solid State Com. **79**, 911 (1991), Surf. Sci. **263**, 346, (1992), A. R. Goñi *et al*, Phys. Rev. Lett. **67**, 3298 (1991).
- [10] J. F. Müller, A. E. Ruckenstein, and S. Schmitt-Rink, Phys. Rev. B **45**, 8902 (1991); T. Ogawa, A. Furusaki, and N. Nagaosa, Phys. Rev. Lett. **24**, 3638 (1992); F. J. Rodriguez and C. Tejedor, Phys. Rev. B **47**, 1506 (1993); **47**, 13015 (1993).
- [11] I. E. Perakis and Y. C. Chang, Phys. Rev. B **47**, 6573 (1993).

- [12] A. Rosch and T. Kopp, Phys. Rev. Lett. **75**, 1988 (1995).
- [13] F. Sols and F. Guinea, Phys. Rev. B **36**, 7775 (1987); K. Vladár, G. T. Zimányi, and A. Zawadowski, Phys. Rev. Lett. **56**, 286 (1986); N. V. Prokof'ev, J. Mosc. Phys. Soc. **2**, 157 (1992); P. Hedegård and A. Caldeira, Phys. Scr. **35**, 609 (1987).
- [14] C.-O. Almbladh and L. Hedin, in *Handbook on Synchrotron Radiation*, ed. by E. E. Koch (North-Holland, 1983), vol. B, p. 611.
- [15] J. B. McGuire, J. Math. Phys. **6**, 432 (1965); **7**, 123 (1966).
- [16] H. Castella and X. Zotos, Phys. Rev. B **47**, 16186 (1993).
- [17] D. M. Edwards, Prog. Theor. Phys. Sup. **101**, 453 (1990); W. von der Linden and D. M. Edwards, J. Phys. C **3**, 4917 (1991).
- [18] S. Sorella, Phys. Rev. B **49**, 12373 (1994).
- [19] S. Sorella, S. Baroni, R. Car, and M. Parinello, Europhys. Lett. **8**, 663(1989).
- [20] E.Y. Loh, J.E. Gubernatis, in *Electrons Phase Transitions*, edited by B.S. Shastry, S.S. Jha, and V. Singh (Springer, Berlin, 1985).
- [21] S. Sorella, A. Parola, M. Parinello, and E. Tosatti, Europhys. Lett. **12**, 721 (1990).
- [22] E. R. Hansen, *A Table of Series and Products* (Prentice Hall Inc., Englewoods Cliffs, N.J., 1975).

FIGURES

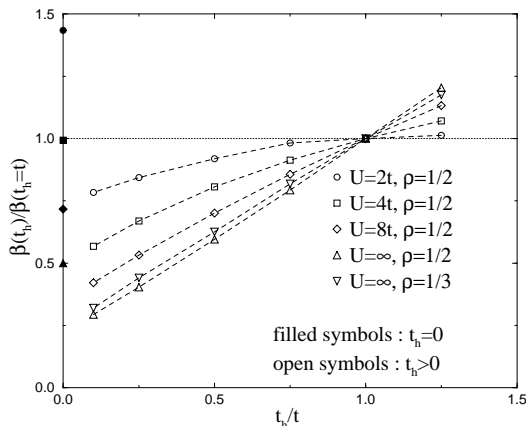


FIG. 1. Exponent $\beta(t_h)/\beta(t_h = 0)$ normalized to the analytical value $\beta(t_h = t)$ in (5) as a function of the mass ratio t_h/t for different interaction strengths U and densities ρ . The filled symbols at $t_h = 0$ are the exact results in(3) for the static impurity. The open symbols for $t_h > 0$ are the exponents extracted as $N \rightarrow \infty$ from the variational results for a sequence of finite systems with $N_1/N_2 = 0.7$, the largest size being $N_1 = 159$ and $N_1 = 121$ at half and third filling, respectively.

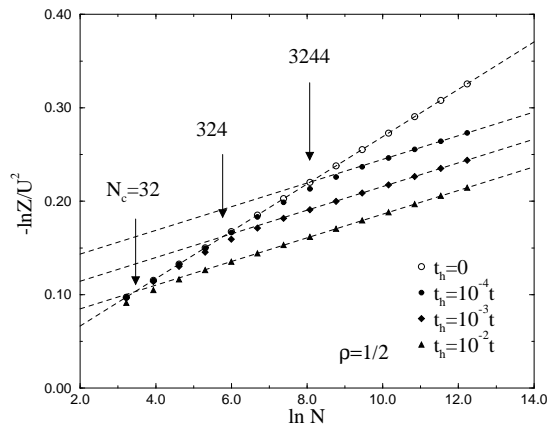


FIG. 2. Logarithmic decay of the quasiparticle weight Z with number of electrons N from the perturbative result in (6) at half filling and for different impurity hopping parameters t_h . The dashed lines are the asymptotic behaviors with the analytical exponent $\beta(t_h)$ in (8). The arrows indicate the estimate of the crossover size N_c from (A10).

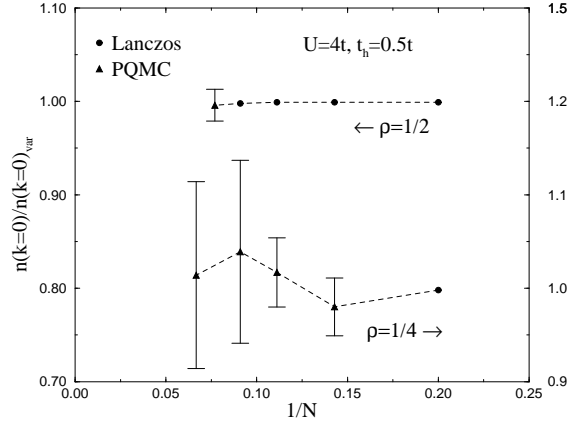


FIG. 3. Ratio of the momentum distribution function $n(k)$ at $k = 0$, calculated with Lanczos diagonalization or Projection Quantum Monte Carlo, to its variational estimate $n(k = 0)_{var}$ as a function of $1/N$ for half and quarter filling and for $U = 4t$, $t_h = 0.5t$. The circles are the Lanczos results and the squares the Monte Carlo results with the corresponding error bars. The left axis refers to half filling and the right axis to quarter filling.

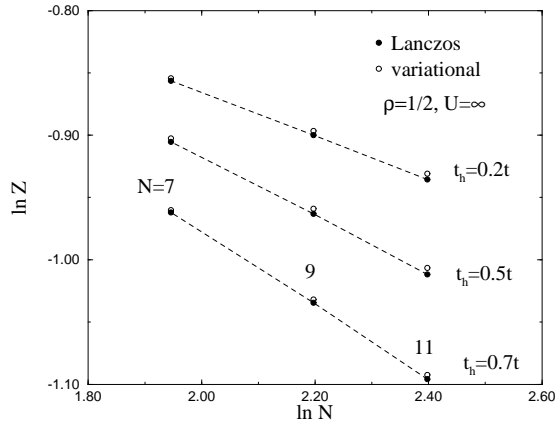


FIG. 4. Comparison of exact spectral weight Z from Lanczos diagonalization to its variational estimate as a function of number of electrons N in log-log plot for $U = \infty$, $\rho = 1/2$ and different t_h . The open symbols are the variational results and the filled symbols Lanczos results.

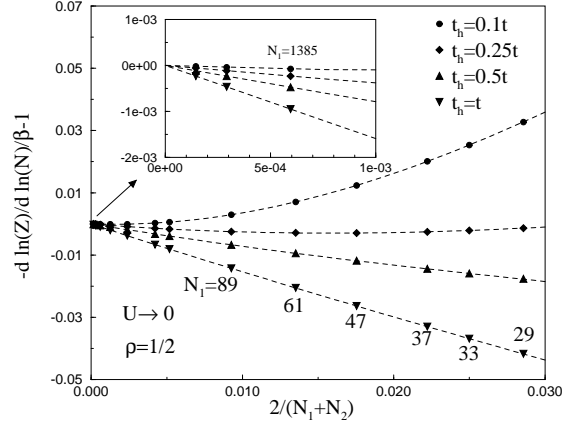


FIG. 5. Slopes $d \ln(Z)/d \ln(N) = (\ln Z_1 - \ln Z_2)/(\ln N_1 - \ln N_2)$ normalized to the analytical value of $\beta(t_h)$ in (8) as a function of the inverse mean number of electrons $2/(N_1 + N_2)$ in the perturbative regime and for different hopping parameters t_h . The spectral weight Z is computed numerically from (6). The dashed lines are numerical fits of the data as polynomials in $2/(N_1 + N_2)$. The inset is a blow-up around the origin.

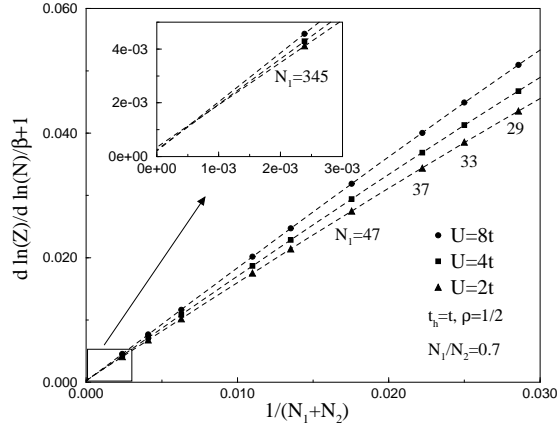


FIG. 6. Slopes $d \ln(Z)/d \ln(N)$ normalized to the analytical value of $\beta(t_h = t)$ in (5) as a function of the inverse mean number of electrons $2/(N_1 + N_2)$ for $t_h = t$ and different interaction strengths $U = 2, 4, 8t$ at half filling and for $N_1/N_2 = 0.7$. The spectral weight Z is computed with the Bethe's ansatz wavefunction in (13). The dashed lines are numerical fits of the data as a third-order polynomial in $2/(N_1 + N_2)$. The inset is a blow-up around the origin.

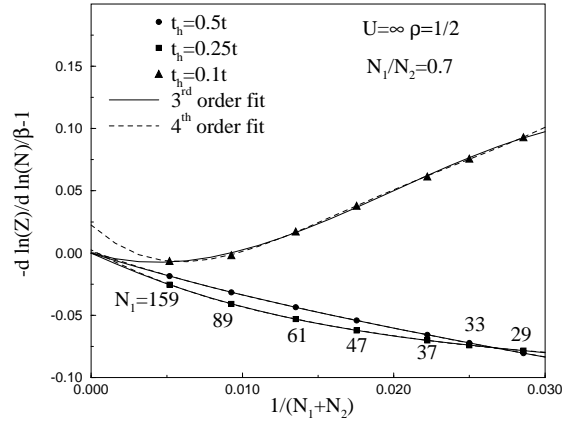


FIG. 7. Slopes $d \ln(Z)/d \ln(N)$ normalized to the fitted $\beta(t_h)$ as a function of the inverse mean number of electrons $2/(N_1 + N_2)$ for $U = \infty$, different hopping parameters $t_h = 0.5, 0.25$ and $0.1t$, at half filling. The spectral weight is computed with the variational wavefunction. The solid and dashed lines are numerical fits of the data as third-order and fourth-order polynomial in $2/(N_1 + N_2)$, respectively.

TABLES

$N (\rho=1/2)$	e_c			$N (\rho=1/4)$	e_c		
	Lanczos	PQMC	variational		Lanczos	PQMC	variational
5	-0.9028		-0.9025	5	-0.6102		-0.6101
7	-0.9230		-0.9227	7		-0.619(4)	-0.6190
9	-0.9340		-0.9336	9		-0.624(3)	-0.6239
11	-0.9408		-0.9404	11		-0.627(2)	-0.6271
13		-0.945(2)	-0.9451	15		-0.632(2)	-0.6309
∞	-0.9727		-0.9720	∞		-0.642(4)	-0.6413

TABLE I. Comparison of correlation energy, $e_c = E_0 - \tilde{E}_0 - U\rho$ where E_0 and \tilde{E}_0 are the ground-state energies of the interacting and noninteracting system, respectively, computed by Lanczos exact diagonalizations, Projection Quantum Monte Carlo (PQMC) and Edwards' variational wavefunction, as a function of the number of fermions N at half and quarter filling ($\rho = N/L = 1/2$ and $1/4$, respectively), for $t_h = 0.5t$, $U = 4t$. The last line gives the energy extrapolated for the infinite system both from either Lanczos or PQMC results and the variational results by a linear fit in $1/N$.